Available online at www.sciencedirect.com
ScienceDirect
Ceramics International 37 (2011) 167–173
CERAMICS INTERNATIONAL
www.elsevier.com/locate/ceramint

Synthesis and characterization of monetite and hydroxyapatite whiskers obtained by a hydrothermal method

Bojan Jokić [a,*], Miodrag Mitrić [b], Velimir Radmilović [c], Sasa Drmanić [a], Rada Petrović [a], Djordje Janaćković [a]

[a] Faculty of Technology and Metallurgy, Karnegijeva 4, 11000 Belgrade, Serbia
[b] Condensed Matter Physics Laboratory, The Vinca Institute, P.O. Box 522, 11001 Belgrade, Serbia
[c] National Center for Electron Microscopy, Lawrence Berkeley National Laboratory, Berkeley, CA 94720, USA

Received 10 June 2010; received in revised form 6 July 2010; accepted 30 July 2010
Available online 21 August 2010

Abstract

High temperature hydrothermal syntheses, using calcium nitrate tetrahydrate, sodium dihydrogen phosphate and urea as precursors, and characterization of hydroxyapatite (HAp) whiskers are reported herein. The morphology and chemical composition of the crystals from a monetite to a hydroxyapatite phase were controlled by varying the starting concentrations of the precursors and the solution pH through the amount of urea that is decomposed during heating. X-ray diffraction (XRD) analysis, infrared spectroscopy (IR), scanning electron microscopy (SEM), energy-dispersive X-ray spectroscopy (EDX), transmission electron microscopy (TEM) and high-resolution TEM (HRTEM) were used to investigate the products of the syntheses in order to find the optimum reaction conditions for obtaining the desired morphology and phase composition. Different morphologies ranging from single crystals of monetite through rods and plates of hydroxyapatite with different size distribution to whisker-like single hydroxyapatite crystal were achieved by simply varying the starting concentration of urea. Structural refinement of the hydroxyapatite whiskers confirmed a strong preferential orientation along the *c*-axis direction of the hexagonal crystal structure, which was significantly different from the usually observed random crystal orientation. TEM and SEM analysis of the apatite whiskers confirmed single crystal structure with the a *c*-axis orientation parallel to the long axis of the whiskers, with sizes up to 150 μm in length, 10 μm in width and with a thickness of about 300 nm, that grew from the same centre of nucleation, forming flaky-like particles.

Keywords: B. Whiskers; D. Apatite; Monetite

1. Introduction

Hydroxyapatite ($Ca_{10}(PO_4)_6(OH)_2$; HAp) has been widely applied as a biomaterial for the substitution of human bone tissues because of its excellent biocompatibility and bioactivity, serving as an alternative to natural bone grafts [1,2]. The inorganic part of human bone and tooth has chemical and structural similarities to Ca-deficient hydroxyapatite, whereas the morphology of HAp can be significantly different in biological tissues, such as plate-like HAp crystals in bone and needle-like hexagonal prisms in enamel [3]. Moreover, the bone mineral crystals also exhibit an elongated *c*-axis (plate shaped) and a preferred orientation in the direction of the principal stress [4]. The intrinsically different surface reactivity of HAp crystals induced by the two types of crystal planes, which bear different charges (a positively charged calcium-rich *c*-surface and a negatively charged hydroxyl- and phosphate-rich *a*-surface), exhibit selective adsorption of various ions, organic compounds, and proteins and therefore becomes an important material for chromatographic uses. In addition, it is expected that HAp whiskers would be a good matrix for gene delivery systems with their biocompatibility and biostability [5,6]. The main limitation of HAp ceramics in orthopedics has been inferior mechanical properties. It is well known that the fracture toughness parameter of HAp is lower than that reported for natural human bones (1 MPa/m^2 compared to 2–12 MPa/m^2) [7] and thus, to date, its applications have been limited to areas where the bones are free of dynamic load, i.e., for non-load

* Corresponding author. Tel.: +381 11 3370 489; fax: +381 11 3370 387.
E-mail address: bjokic@tmf.bg.ac.rs (B. Jokić).

0272-8842/$36.00
doi:10.1016/j.ceramint.2010.08.032

bearing, craniofacial and periodontal applications, for coatings [8] or as materials for the scaffolds used for bone tissue engineering [7,9,10].

One of the most studied methods to improve the mechanical properties of HAp ceramics and calcium-phosphate cements is the addition of whiskers [10]. Investigations of HAp with a rod-like morphology have attracted much attention during the past few years because of the proved decrease in biocompatibility and bioactivity when fibrous bio-inert materials, such as SiC, C, Si_3N_4, Al_2O_3 or ZrO_2, were used for bioceramic reinforcement [11,12]. In reinforced polymers, the use of aligned HAp whiskers instead of HAp powder resulted in an improved stiffness, strength and toughness and an anisotropy more like that found in human cortical bone tissue [13]. HAp whiskers have been synthesized by various methods, mainly by hydrothermal synthesis [14–16] using wet-chemically prepared HAp precursors of low crystallinity and irregular morphology or using gels as the starting materials [17,18], homogeneous precipitation [19], molten salts synthesis [20], and by liquid–solid–solution synthesis [21]. The whiskers or fibers prepared by the solid reaction and in the gel system showed a sensitive dependence on the preparation conditions, and their crystallinity and thermal stability were relatively inferior. Homogenous precipitation with a slow reaction rate is a relatively easy procedure for obtaining uniform HAp particles, but many precipitated fibrous HAp prepared with a wide range of compositions and under a wide variety of experimental conditions had a relatively low crystallinity and were not a pure HAp phase with a low aspect ratio [22–25].

The aim of the present work was to find the optimum reaction conditions for the synthesis of monetite and hydroxyapatite with defined morphology by varying the starting concentration of the precursors and the pH value of the solution. This synthesis procedure takes advantage of the fact that a gradual increase up to different final pH values, controlled by the concentration of urea, allow pure monetite and hydroxyapatite single crystals phases with controlled morphology and size to be obtained.

2. Materials and methods

2.1. Synthesis of monetite powder and hydroxyapatite whiskers

Apatite crystals with different morphology were synthesized by a modified hydrothermal method at high temperature *via* the direct reaction between calcium nitrate tetrahydrate ($Ca(NO_3)_2{\bullet}4H_2O$, 99.8%, Carlo Erba) and sodium dihydrogen phosphate dihydrate ($NaH_2PO_4{\bullet}2H_2O$, Carlo Erba) using urea ($(NH_2)_2CO$, Fluka) as a homogeneous precipitation agent [26,27]. Each synthesis was performed by mixing stoichiometric amounts of $Ca(NO_3)_2{\bullet}4H_2O$ and $NaH_2PO_4{\bullet}2H_2O$ (Ca/P = 1.67) and varying amounts of urea in 1500 ml of distilled water in a glass vessel. In order to provide uniform thermal transport, 1500 ml of distilled water was placed in the gap between the glass vessel and the stainless-steel vessel. The reaction temperature was measured by a thermocouple placed inside a thermo well in the vessel. The initial pH value of the suspension was 4.5 for all synthesis conditions without adjustment with an acid. The autoclave was heated up to 160 °C during 1 h and kept at this temperature for 2 h. After this period, autoclave was left to cool down slowly in 10 h to room temperature. The formed HAp precipitates were collected from the solution by vacuum filtration and washed with distilled water.

2.2. Characterization

The diffraction patterns of the polycrystalline samples (A1, A2 and A3) were measured using a conventional powder diffractometer (Philips PW 1050) with Bragg–Brentano geometry and Cu $K_{\alpha 1,2}$ radiation (Ni filter). The diffractograms were recorded at room temperature in the 2Θ range 5–70° with a 2Θ step of 0.02° and a counting time of 2 s per data point (for sample A4 in the 2Θ range 8–120° with a 2Θ step of 0.02° and a counting time of 14 s per data point). A 1/2° source slit and a 0.1 mm receiving slit were used.

The crystal structure refinement was based on the Rietveld full profile method using a Koalariet computing program based on the Fundamental Parameters convolution approach to generate the line profiles [28,29]. This program is appropriate for processing data obtained from samples with dominant microstructure parameters [29]. The morphology of the obtained powders was studied by scanning electron microscopy (SEM) using a Jeol JSM-5800 at 20 kV and an FIB SEM at 5 kV, transmission electron microscopy (TEM), electron diffraction (ED) and high-resolution TEM (HRTEM) using conventional TEM at 200 kV Jeol 200CX and HRTEM at 80 kV. Prior to SEM analysis, the powder samples were coated with gold using a splutter coater. The chemical composition of the samples was analyzed using an energy-dispersive spectrometer, EDS, with a SiLi X-ray detector (Oxford Instruments, UK) connected to a scanning electron microscope and a computer multi-channel analyzer. The measurements were performed to detect P and Ca. Fourier transform infrared spectroscopy (FTIR) was performed using a MB Bomen 100 Hartmann and Braun spectrometer in the wave number range from 400 to 4000 cm^{-1}. The crystalline products (≈3 mg) were thoroughly ground with (≈500 mg) potassium bromide powder (KBr for IR, Merck) in an agate mortar to homogenize the mixture.

3. Results and discussion

Hydroxyapatite crystals with different morphology were prepared by the direct reaction between $Ca(NO_3)_2{\cdot}4H_2O$ and Na_2HPO_4 under hydrothermal conditions at 160 °C. The initial concentrations of the starting reagents are given in Table 1. Four syntheses were performed with same Ca/P ratio 1.67, while the concentration of urea varied.

The powder XRD patterns of the synthesized samples are shown in Fig. 1, from which the phase composition was determined. It can be observed that sample A1 presented a pure monetite phase. In XRD pattern, all the peaks are in a good

Table 1
Parameters of hydroxyapatite and monetite synthesis.

Sample	Concentration (g)			Ca/P (mol)	$pH_{initial}$	pH_{final}	Phase composition	Particles morphology
	$Ca(NO_3)_2{\bullet}4H_2O$	$NaH_2PO_4{\bullet}2H_2O$	Urea					
A1	15.17	6.00	0.5	1.01	4.5	3.1	Monetite	Large pinacoidal and rod-like crystals
A2	15.17	6.00	1	1.15	4.5	4.2	Monetite, hydroxyapatite	Rod-like crystals
A3	15.17	6.00	2	1.42	4.5	5.7	Hydroxyapatite, monetite	Plate and rod-like crystals
A4	15.17	6.00	3	1.65	4.5	6.9	Hydroxyapatite	Whiskers

agreement with standard (JCPDS card number 70-1425). A gradual increase of the pH value due to the higher concentration of urea led to the formation of a small amount of hydroxyapatite phase in sample A2, which is evident from its diffractogram (Fig. 1). A further increase of the amount of urea resulted in the formation an almost pure hydroxyapatite phase (JCPDS card number 09-9432), observed in samples A3 and A4 (Fig. 1). The highly crystalline structure of all the products can be distinguished. The peaks on the diffractogram, corresponding to the prism planes (1 0 0), (2 0 0) and (3 0 0), are strong and sharp in the sample A4, which was synthesized with the highest concentration of urea in the starting solution.

The formation mechanism of monetite and HAp whiskers can be explained as follows. Namely, monetite as the more stable phase under acidic condition below pH 2.7 was formed first. Increasing the amount of urea in the starting solution led increases in the pH value of the solution due to urea decomposition. At elevated temperatures, above 80 °C, $(NH_2)_2CO$ continuously decomposes to form carbon dioxide and aqueous ammonia species. In turn, such *in situ* released NH_3(aq) gradually increased the pH of the reaction solution to values wherein HAp becomes the more thermodynamically stable calcium orthophosphate compound (i.e., less soluble) and is thus formed. With increasing pH value, the hydroxyapatite phase was formed as the more stable phase at pH >4.8 [30,31].

3.1. Structure refinement of HAp whiskers

The X-ray powder diffraction pattern of the A4 sample was used for structural refinement. It can be observed that this pattern, due to strong preferential crystallite orientation (Fig. 2), significantly differed from the usually obtained patterns of HAp with a random crystallite orientation [20]. No evident violations of hexagonal symmetry were found on the X-ray diffraction pattern of the sample. Therefore, the refinement of the structure was performed in the space group $P6_3/m$ in the well-known apatite type crystal structure with following crystallographic ion positions [28]: Ca^{2+} located at two crystallographic positions – one at 6h [xy1 = 4] with the local symmetry m and the other at the position 4f [1/3 2/3 z] with the local symmetry 4f; P^{5+} located at the crystallographic position 6h [xy1 = 4] with the local symmetry m; O^{2-} located at two different 6h positions [xy1 = 4] with the local symmetry m, and at the general crystallographic position 12i [xyz] with the local symmetry 1; OH^- located at the crystallographic position 2a [0 0 1/4] with the local symmetry %6. The starting atomic parameters for this structure were taken from the refinement in the space group $P6_3/m$ obtained using neutron single crystal data [32]. The atom positions, unit cell, background, crystal size, micro-strain displacement parameters, thermal B factor and preferential orientation were allowed to vary. All these parameters obtained by refinement are given in Table 2.

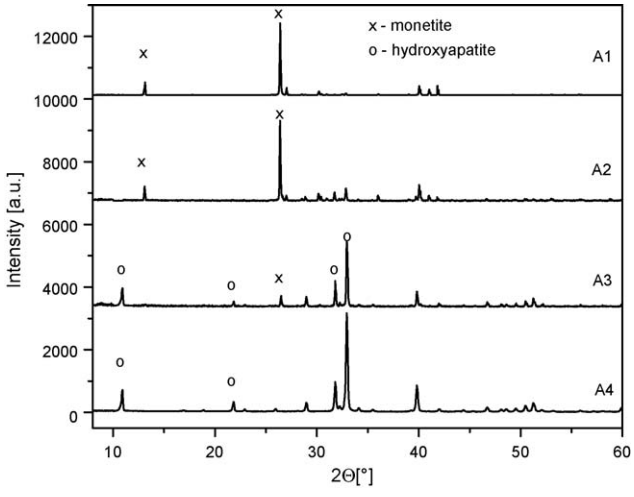

Fig. 1. X-ray diffractograms collected from the hydrothermal synthesized products.

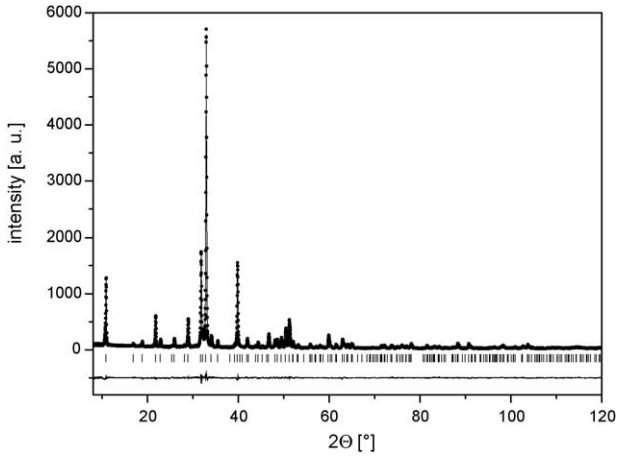

Fig. 2. The observed (•), calculated (–) and difference (bottom) X-ray diffraction data of the A4 sample taken at room temperature. Vertical markers below the diffraction patterns indicate the positions of possible Bragg reflections.

Table 2
The results of the structural refinement for hydroxyapatite whiskers (sample A4).

	x	y	z	B (Å^2)
Ca^{2+} (6h)	0.2518(2)	0.9939(3)	1/4	0.91(4)
Ca^{2+} (4f)	1/3	2/3	0.4898(7)	0.83(5)
P^{5+} (6h)	0.4033(3)	0.3746(3)	1/4	1.00(6)
O^{2-} (1) (6h)	0.3364(4)	0.4751(5)	1/4	0.5(1)
O^{2-} (2) (6h)	0.5961(7)	0.4398(7)	1/4	1.7(1)
O^{2-} (3) (12i)	0.3254(3)	0.2595(4)	0.4383(7)	4.2(1)
OH^-	0	0	1/4	1.9(2)

Lattice parameters [Å]	a = 9.44415(6) c = 6.8913(26)
Crystal size [nm]	329(18)
Micro-strain [%]	0.133(5)
Preferential orientation	0.4960
R_{wp} [%]	8.8

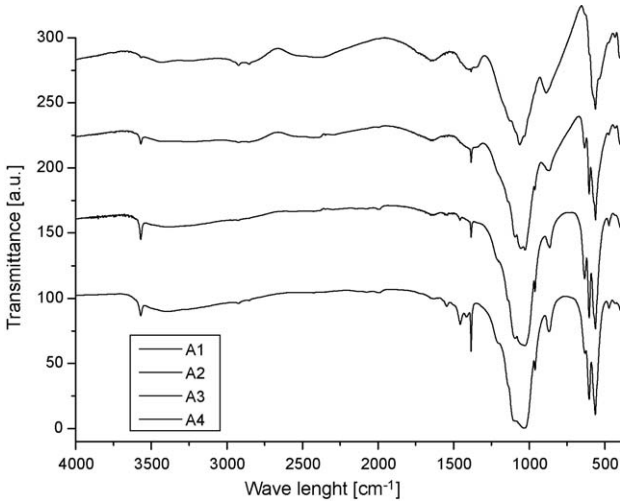

Fig. 3. IR spectra of the hydrothermally synthesized products.

The crystal structure refinement showed a very developed preferential orientation of the HAp whiskers (collected in the reflection mode), which was the cause of the clearly observed differences between the diffractogram of the obtained HAp whiskers and that of HAp with a random crystallite orientation [20]. In addition, as can be observed on the diffractogram (Fig. 2), very intensive reflections arose from plane close to the 1 0 0 direction, which masked the reflections along the 0 0 1 direction. Every attempt to prepare a sample in order to obtain a random distribution of crystallites was ineffective. This probably means that whiskers overgrow along the *c*-axis are arranged naturally in such a way that the plane placed along 0 0 1 direction are lined out perpendicular to the surface of the sample. The calculated size of the crystallites and TEM microphotographs indicate that the thickness of the whiskers

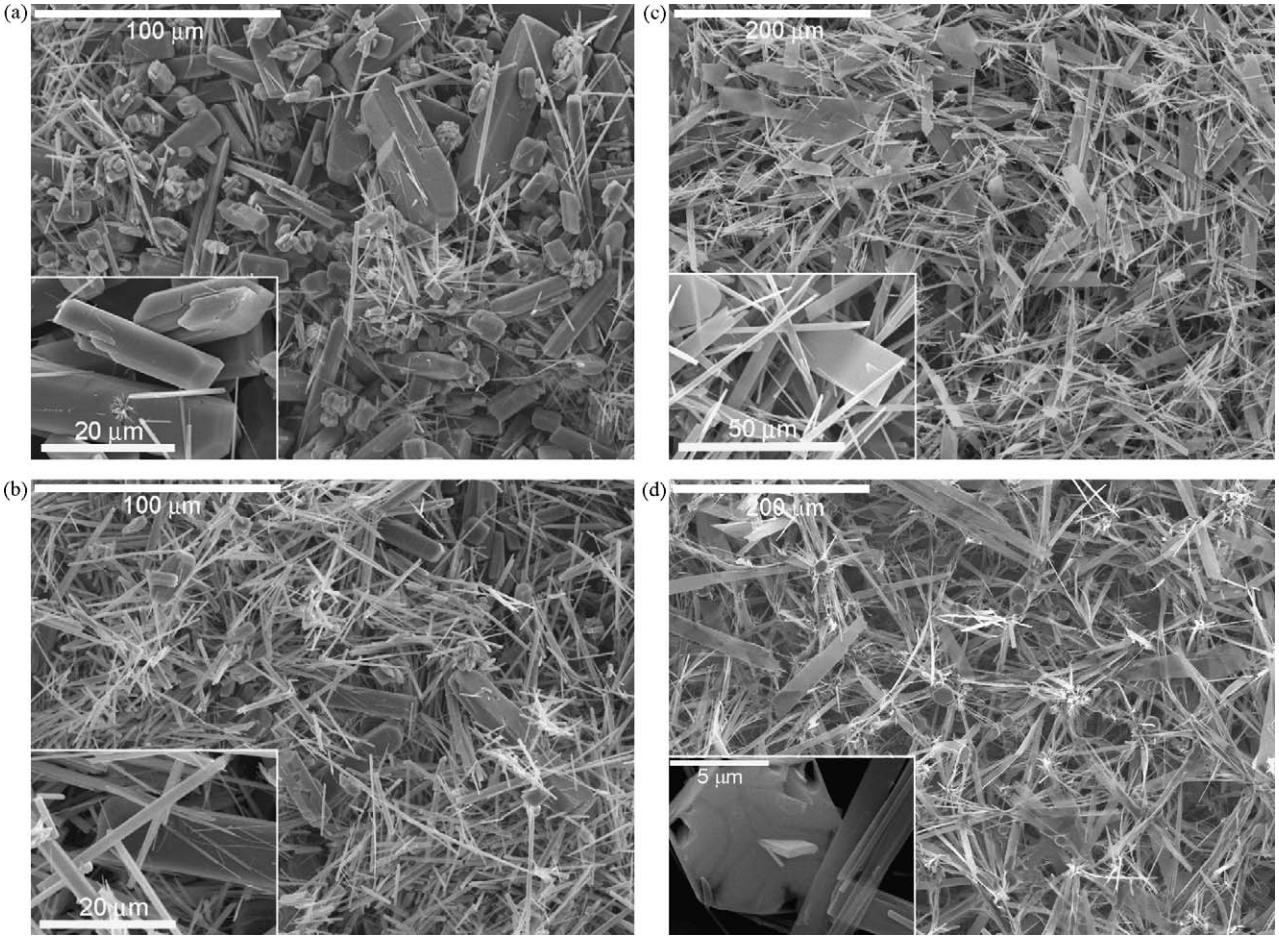

Fig. 4. SEM microphotographs of hydrothermal prepared samples with high magnification insets: (a) A1, (b) A2, (c) A3) and (d) A4.

was around 300 nm. Otherwise, evidence that the half width at half maximum of the peaks on the diffractogram were not significantly changed from those of crystal systems in which the crystallites were developed along the *c*-axis, indicating that the crystallites had the same dimensions in all directions.

The FTIR spectra of the hydrothermally synthesized products are shown in Fig. 3. These spectra confirm the functional groups present, which provides information about the phase purity of the sample synthesized under different pH conditions.

The OH liberation mode at 630 cm^{-1} can be clearly seen in the spectra of the A3 and A4 samples. The broad OH stretching band of water from 2800 to 3600 cm^{-1} can be observed in the spectra of all the samples, while the water bending mode at 1640 cm^{-1} is more expressed in the spectrum of the A1 sample. The ν_1 PO_4 band, occurring at 960 cm^{-1}, is observed in the FTIR spectra of the A2, A3 and A4 samples. The triple degeneracy of the ν_3 PO_4 mode at ≈1070 cm^{-1} is not seen in the spectra of samples A3 and A4 because the band is too strong. The bands at 1025, 1100 and the weak band at 1145 cm^{-1} were assigned to HPO_4^{2-} ions and it can be observed that the band at 1025 cm^{-1} is more expressed in the spectra of the A1 and A2 samples. In addition, the intensity of the band at 875 cm^{-1}, assigned to the acidic phosphate group (HPO_4^{2-}), decreased with increasing amount of HAp whiskers present in the powders. In the study of ν_4 PO_4, the two bands at 530 and 550 cm^{-1} on the low frequency side of $\nu 4$ were assigned to HPO_4^{2-}. Bands at 1545 and 1450 cm^{-1}, arising from CO_3^{2-} ions that replaced some of the OH^- ions (A-type), are visible in the spectra of A3 and A4. Considering the spectrum of the A3 and A4 samples, it can be concluded according to the bands which appeared at 1412 and 873 cm^{-1} that the major fraction of the PO_4^{3-} ions (B-type) had been replaced by CO_3^{2-}. Additionally, in the spectra of the A3 and A4 samples, the increase in intensity of the band at ≈1450 cm^{-1} was greater than the increase in the intensity of the band at ≈1542 cm^{-1} [33]. Hence, all four hydrothermally derived samples are AB-type carbonated hydroxyapatite. These carbonate anions are believed to arise from the decomposition of urea.

Detailed microstructural studies using SEM and TEM gave further insight into the shape and size of the formed phases.

The SEM morphologies of the synthesized powders are shown in Fig. 4. Fig. 4a shows well-developed crystals of monetite of ≈10–80 μm in length and ≈5–20 μm in width. In the same microphotographs, smaller rod-like crystals of monetite are also observed. On increasing the amount of urea (Fig. 4b), the rod-like form of the obtained monetite crystals became the dominant crystal form. The further increase of the urea content in the starting solution led to the formation of the HAp phase that is characterized by plate-like crystal shapes (Fig. 4c). The large pinacoidal crystals of monetite present in the samples A1 and A2 (Figs. 4a, b) are not visible in the microphotographs of sample A3, although XRD analysis confirmed the presence of a small amount of monetite. In order to increase the quantity of hexagonal whiskers, a gradual increase of the pH of the reaction medium was realized by the addition of more urea to the solution. The formation of flake-like particles of pure HAp phase, collected from the bottom of the glass vessel, composed of a large number of whiskers, can be observed in the microphotographs presented in Fig. 4d. This SEM observation shows they are ≈50 and 150 μm in length, ≈2 and 10 μm in width. In the same microphotographs, the presence of cup-like particles with 6th order axes could be seen in the centre of the flaky particles (Fig. 4d) and in isolation (Fig. 4d inset). Their formation could be explained by the Wulf shape theory, which determines the equilibrium shape of a perfect crystal of one material in contact with a single surrounding medium. The equilibrium shape is determined by minimizing the total system energy, which is composed of contributions from the bulk and surface of the crystal [34].

The whisker morphology of the flaky-like particles of HAp collected from the middle of the glass vessel is shown in Fig. 5a. It can be observed in the microphotograph (Fig. 5a inset) that the above-mentioned hexagonal cup-like form is found in the centre of the flaky particles. The hydroxyapatite whiskers are formed from hexagonal cups as a consequence of the fast growing rate of HAp along the *c*-axis (Fig. 4d inset). A high magnification microphotograph of the same sample (Fig. 5b) shows that the average whisker thickness is about 300 nm, which was confirmed by the Rietvald refinement of the crystal structure. When the

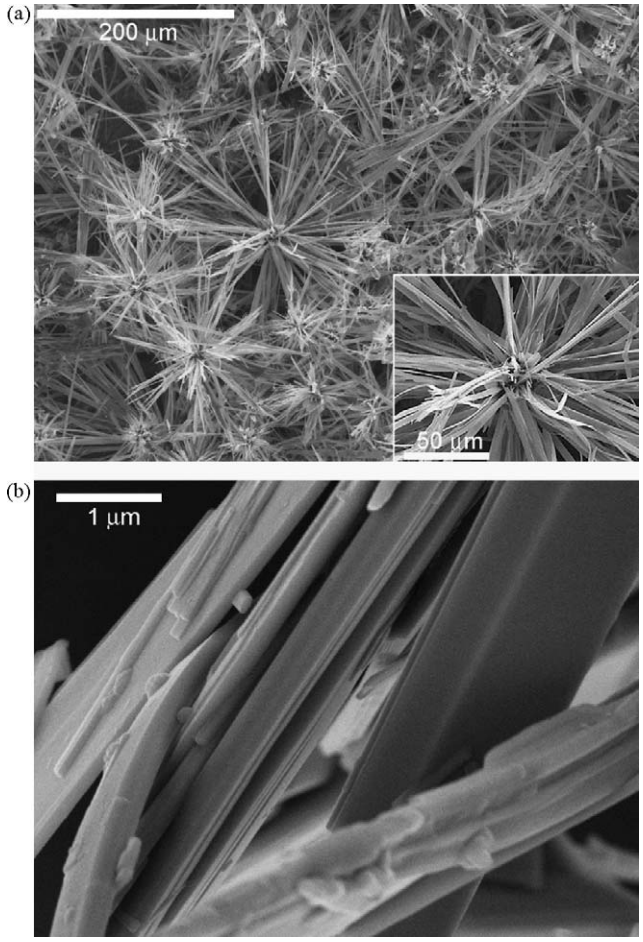

Fig. 5. SEM microphotographs of hydrothermally prepared HAp whiskers (sample A4): (a) low and (b) high magnification.

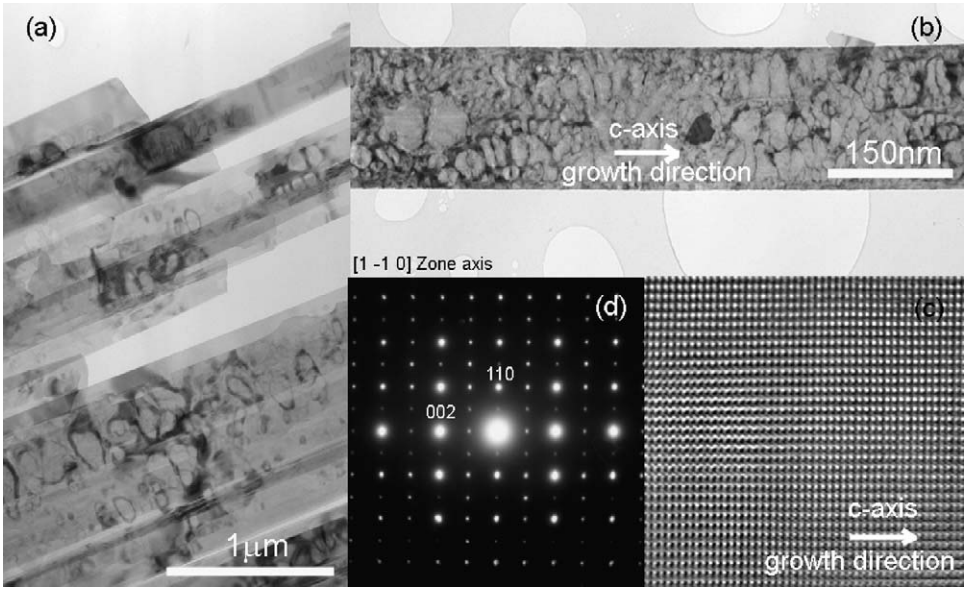

Fig. 6. Low magnification TEM image of sample A4 (a); TEM image of the HAp whiskers (b); HRTEM image of the HAp whiskers with the lattice plane visible (c) and the corresponding ED pattern of HAp whiskers (d).

hydrothermal syntheses were performed at higher temperatures, intensive decomposition of urea occurred, generating a large number of nuclei, which should induce the formation of smaller crystals. Despite these predictions, only highly crystalline HAp powders with elongations of up to 150 μm were obtained.

Transmission electron microscopy was applied to investigate the microstructure of the whiskers. A low magnification TEM image of dried whiskers of sample A4 is shown in Fig. 6 inset a. The electron diffraction pattern corresponding to the centre of the whiskers is shown in Fig. 6 inset d. The electron diffraction pattern indicates that the whiskers are single crystals, which was also confirmed by XRD analysis. The spots of the electron diffraction pattern can be completely indexed in the HAp hexagonal $P6_3/m$ space group using the HAp cell parameters of JCPDS card number 09-9432 (Fig. 6 inset c). A representative HRTEM image along the [1 1 0] zone axis is given in Fig. 6 inset c, which confirms the perfect hydroxyapatite structure of the A4 sample. TEM/ED/HRTEM analysis confirms the previous conclusion derived from XRD structure refinement that the whiskers of the sample A4 are single crystals oriented with their axis along the *c*-axis.

4. Conclusions

Hydroxyapatite whiskers were successfully synthesized by the hydrothermal method using $Ca(NO_3)_2{}^{\bullet}4H_2O$, $(NH_4)_2HPO_4{}^{\bullet}2H_2O$ and urea. The obtained products were flaky-like hydroxyapatite particles composed from whiskers that are formed from the centre of hexagonal cup-like particles. Moreover, structural refinement of the hydroxyapatite whiskers determined a strong preferential orientation along the *c*-axis direction of the hexagonal crystal structure significantly different from the usually observed random crystal orientation. Individual TEM analysis of the apatite whiskers confirmed the single crystal structure with the *c*-axis orientation parallel to the long axis of the fibers. It was also registered by FTIR spectroscopy that the hydroxyapatite whiskers had partial substitution of both PO_4^{3-} and OH^- groups by carbonate anions. Hydroxyapatite and monetite crystals with different morphologies and size distributions could be obtained by controlling the final pH value of the solution by the addition of different amounts of urea to the starting solution.

Acknowledgements

The authors wish to acknowledge the financial support from Ministry of Science and Technological Development of the Republic of Serbia through the projects 142070B and EUREKA E! 3033 Bionanocomposit.Transmission electron microscopy characterization was performed at the National Center for Electron Microscopy, Lawrence Berkeley National Laboratory, supported by the Director, Office of Science, Office of Basic Energy Sciences, Materials Sciences and Engineering Division, of the U.S. Department of Energy under Contract No. DE-AC02-05CH11231.

References

[1] L.L. Hench, J. Wilson, An Introduction to Bioceramics, World Scientific Publishing, 1998.
[2] H. Oguchi, K. Ishikawa, K. Mizoue, K. Seto, G. Eguchi, Long-term histological evaluation of hydroxyapatite ceramics in humans, Biomaterials 16 (1995) 33–38.
[3] D. Walsh, J.L. Kingston, B.R. Heywood, S. Mann, Influence of monosaccharides and related molecules on the morphology of hydroxyapatite, J. Cryst. Growth 133 (1993) 1–12.
[4] R. Wenk, F. Heidelbach, Crystal alignment of carbonated apatite in bone and calcified tendon: results from quantitative texture analysis, Bone 24 (1999) 361–369.

[5] T. Kawasaki, Hydroxyapatite as a liquid chromatographic packing, J. Chromatogr. 544 (1991) 147–184.
[6] K. Ioku, S. Yamauchi, H. Fujimori, S. Goto, M. Yoshimura, Hydrothermal preparation of fibrous apatite and apatite sheet, Solid State Ionics 151 (2002) 147–150.
[7] J.E. Barralet, L. Grover, T. Gaunt, A.J. Wright, I.R. Gibson, Preparation of macroporous calcium phosphate cement tissue engineering scaffold, Biomaterials 23 (2002) 3063–3072.
[8] L.L. Hench, Bioceramics, from concept to clinic, J. Am. Ceram. Soc. 74 (1991) 1487–1510.
[9] V. Karageorgiou, D. Kaplan, Porosity of 3D biomaterial scaffolds and osteogenesis, Biomaterials 26 (2005) 5474–5491.
[10] F.A. Müller, U. Gbureck, T. Kasuga, Y. Mizutani, J.E. Barralet, U. Lohbauer, Whisker-reinforced calcium phosphate cements, J. Am. Ceram. Soc. 90 (2007) 3694–3697.
[11] K. Hark, S. Sundaresan, T. Vasilos, C. Sung, SiC whisker- and C fiber-reinforced calcium phosphate composites, J. Mater. Res. 9 (1994) 2476–2479.
[12] A.J. Ruys, M. Wei, M.B.K. Milthorpe, A. Brandwood, C.C. Sorrell, Hydrothermal sintering of ZrO_2 and Al_2O_3 fiber-reinforced hydroxyapatite, J. Aust. Ceram. Soc. 29 (1993) 39–49.
[13] R.K. Roeder, M.M. Sproul, C.H. Turner, Hydroxyapatite whiskers provide improved mechanical properties in reinforced polymer composites, J. Biomed. Mater. Res. A 67 (2003) 801–812.
[14] M. Yoshimura, H. Suda, K. Okamoto, K. Ioku, Hydrothermal synthesis of biocompatible whiskers, J. Mater. Sci. 29 (1994) 3399–3402.
[15] I.S. Neira, F. Guitian, T. Taniguchi, T. Watanabe, M. Yoshimura, Hydrothermal synthesis of hydroxyapatite whiskers with sharp faceted hexagonal morphology, J. Mater. Sci. 43 (2008) 2171–2178.
[16] M.A. Verges, C.F. Gonzalez, M.M. Gallego, Hydrothermal synthesis of calcium deficient hydroxyapatites with controlled size and homogeneous morphology, J. Eur. Ceram. Soc. 18 (1998) 1245–1250.
[17] Y. Mizutania, M. Hattoria, M. Okuyamaa, T. Kasugab, M. Nogamib, Large-sized hydroxyapatite whiskers derived from calcium tripolyphosphate gel, J. Eur. Ceram. Soc. 25 (2005) 3181–3185.
[18] R.K. Roeder, G.L. Converse, H. Leng, W. Yue, Chelate decomposition method kinetic effects on hydroxyapatite whiskers synthesized by the chelate decomposition method, J. Am. Ceram. Soc. 89 (7) (2006) 2096–2104.
[19] M. Aizawa, H. Ueno, K. Itatani, I. Okada, Syntheses of calcium-deficient apatite fibres by a homogeneous precipitation method and their characterizations, J. Eur. Ceram. Soc. 26 (2006) 501–507.
[20] C. Tas, Molten salt synthesis of calcium hydroxyapatite whiskers, J. Am. Ceram. Soc. 84 (2001) 295–300.
[21] X. Wang, J. Zhuang, Q. Peng, Y.D. Li, Liquid–solid–solution synthesis of hydroxyapatite nanorods, Adv. Mater. 18 (2006) 2031–2034.
[22] S. Suzuki, M. Ohgaki, M. Ichiyanagi, M. Ozawa, Preparation of needle-like hydroxyapatite, J. Mater. Sci. Lett. 17 (1998) 381–383.
[23] K. Kandori, N. Horigami, A. Yasukawa, et al., Texture and formation mechanism of fibrous calcium hydroxyapatite particles prepared by decomposition of calcium-EDTA chelates, J. Am. Ceram. Soc. 80 (1997) 1157–1164.
[24] .A. Yasukara, H. Takase, K. Kandori, et al., Preparation of calcium hydroxyapatite using amides, Polyhedron 13 (1994) 3071–3078.
[25] H. Zhang, Y. Wang, Y. Yan, S. Li, Precipitation of biocompatible hydroxyapatite whiskers from moderately acid solution, Ceram. Int. 29 (2003) 413–418.
[26] Dj. Janackovic, I. Petrovic-Prelevic, Lj. Kostic-Gvozdenovic, R. Petrovic, V. Jokanovic, D. Uskokovic:, Influence of synthesis parameters on the particle sizes of nanostructured calcium-hydroxyapatite, Key Eng. Mater. 203 (2001) 192–195.
[27] Dj. Janackovic, I. Jankovic, R. Petrovic, Lj. Kostic-Gvozdenovic, S. Milonjic, D. Uskokovic:, Surface properties of HAP particles obtained by hydrothermal decomposition of urea and calcium-EDTA chelates, Key Eng. Mater. 437 (2003) 240–242.
[28] H.M. Rietveld, A profile refinement method for nuclear and magnetic structures, J. Appl. Cryst. 2 (1969) 65–71.
[29] R.W. Cheary, A.A. Coelho, A fundamental parameters approach to X-ray line-profile fitting, J. Appl. Crystallogr. 25 (1992) 109–121.
[30] I.S. Neira, Y.V. Kolenko, O.I. Lebedev, G. Tendeloo, H.S. Gupta, F. Guitian, M. Yoshimura, An effective morphology control of hydroxyapatite crystals via hydrothermal synthesis, Cryst. Growth Des. 9 (2009) 466–474.
[31] E. Fernandez, F.J. Gil, M.P. Ginebra, F.C. Driessens, J.A. Planell, S.M. Best, Calcium phosphate bone cements for clinical applications Part I. Solution chemistry, J. Mater. Sci. Mater. Med. 10 (1999) 169–176.
[32] K. Sudarsanan, R.A. Young, Significant precision in crystal structural details: Holly Springs hydroxyapatite, Acta Crystallogr. B 25 (1969) 1534–1543.
[33] J.C. Elliott, Structure and Chemistry of the Apatitets and other Calcium Orthophosphates, Elsevier, 1994, pp. 169–179.
[34] D. Peng, S. Osher, B. Merriman, H.K. Zhao, The geometry of Wulf crystal shapes and its relations with riemann problems, Contemp. Math. 238 (1999) 251–303.